Quantifying nanoscale biochemical heterogeneity in human epithelial cancer cells using combined AFM and PTIR absorption nanoimaging.

Eamonn Kennedy[*1], Rasoul Al-Majomaie[1,2,3], Mohammed Al-Rubeai[2], Dominic Zerulla[1,4], James H. Rice[1]*

Nanophotonics Research Group, School of Physics, University College Dublin, Belfield, Dublin, Ireland e-mail: James.rice@ucd.ie [3]

[1]School of Physics, University College Dublin, Belfield, Dublin, Ireland
[2]School of Chemical and Bioprocess Engineering, University College Dublin, Ireland
[3]Institute of Laser for Postgraduate Studies, University of Baghdad, Iraq
[4]Department of Engineering, University of California Berkeley - Berkeley, CA, USA

Received zzz, revised zzz, accepted zzz
Published online zzz

Key words: Atomic Force Microscopy (AFM), Photothermal Induced Resonance (PTIR), infrared spectral imaging, colon cancer nanotechnology, subcellular imaging

Subcellular chemical heterogeneity plays a key role in cell organization and function. However the biomechanics underlying the structure-function relationship is governed by cell substructures which are poorly resolved using conventional chemical imaging methods. To date, advances in sub-diffraction limited infrared (IR) nanoscopy have permitted intracellular chemical mapping. In this work we report how image analysis applied to a combination of IR absorption nanoimaging and topographic data permits quantification of chemical complexity at the nanoscale, enabling the analysis of biochemical heterogeneity in mammalian cancer cells on the scale of subcellular features.

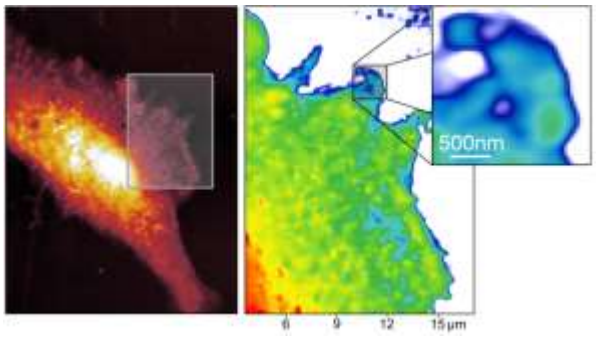

Cell topography and a chemical complexity map of a cancer cell subsection, illustrating biochemical heterogeneity localized with nanoscale resolution.

1. Introduction

Chemical heterogeneity on the micro and nanometre length scales is a key feature of living systems [1]. On the cell membrane, the spatiotemporal confinement of proteins and lipids which govern cell adhesion, signalling and cell-cell interactions occur in specific, submicron geometries [2]. While the association between lipids and proteins within these microdomains directly affects biological functions and dynamic cell processes, their relationship is poorly understood in part due to the current limitations on nanoscale localization of membrane features [3]. Research into this topic has suggested that lipid rafts are involved, with diameters from 20-100 nm, a range which makes their direct visualization challenging using conventional microscopy [4]. Hinterdorfer et al [2] note the importance of plasma membrane heterogeneity for function as any factor that influences the structure of a cell can also alter its mechanical and chemical properties [5]. Similar work has led to a growing recognition that mechanical factors crucially influence cell function, and are involved in numerous diseases including cancer [6].

As the biomechanics underlying the structure-function relationship is governed by cell substructures (which in-

* Corresponding author: Eamonn.kennedy@ucdconnect.ie Phone: +00 353 1716 1735,

fluence cell function through dynamically mediated load-bearing [7]), they can adversely affect function when inhibited, *e.g.* by a decrease in cell motility and migration [8]. Therefore quantifying the underlying biochemical heterogeneity and cytomorphology of subcellular features is of key interest in understanding disease and realizing advances in diagnostics and therapeutics.

Probe-based multimodal, tip-hybridized and force mapping methods enable cellular analysis on the scale of fully resolved cell substructures [9]. Atomic Force Microscopy (AFM) [10] has had tremendous success in answering complex questions in biology [11] brought about by its ability to image both in air and in buffer solutions (aqueous or non-aqueous) over a wide range of temperatures and down to atomic resolution. In spite of having similar overall morphology, researchers have so far detected malignant transformation and discriminated the mechanical properties of tumour and control cell populations with AFM [12]. Despite having demonstrated imaging of pathogens and cancer, scanning probe based tools have not seen wide use in mainstream biological research, in part due to the persistent difficulties associated with imaging soft, live cells in situ. Additionally, there is a need for methods which are non-destructive, yet capable of chemical specific nanoimaging in situ.

One such method, IR nanospectroscopic absorption imaging [13], is based on detection of photothermal induced resonance (PTIR), which can perform spectroscopic mapping and label free chemical identification of cell components on the nanoscale. The technique (also referred to as AFM-IR) is based on the fact that a small, sensitive cantilever placed in contact with the sample surface during pulsed photothermal excitation will be displaced with a magnitude proportional to the material absorption coefficient at the excitation wavelength. [14, 15]. Although the cantilever deflection is proportional to the light absorbed, PTIR measurements provide only an indirect measurement of absorption, as the signal obtained also depends on the physical and thermal properties of the contact material [16]. In terms of physical properties, we would expect soft materials to elicit higher deflections as a result of the local elastic coefficients involved. Similarly, the thermal properties of the material, which include thermal conductivity, thermal capacitance (which is itself a function of temperature and material phase) and critically, the thermal expansion coefficient can also limit the accuracy of the spectral measurements, especially in heterogeneous media where the local sample properties are challenging to precisely define.

However, where these properties are approximately invariant as a function of wavelength and position, spectra and infrared maps of the local absorption co-efficient can be obtained. This has led to the use of the PTIR technique for absorption imaging and spectroscopy of numerous biomaterials, including lipids [17], proteins [18], bacteria [19] and live cells [20]. When probing small features such as viruses within a host organism [21], the power of the method for discriminating heterogeneous chemical signals far below the optical diffraction limit becomes apparent.

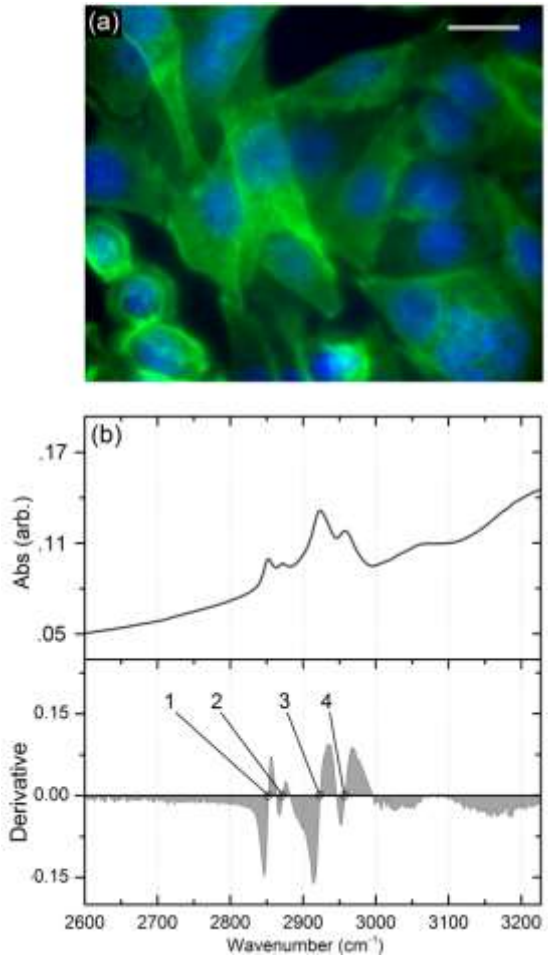

Figure 1 Cell characterization. The fixation quality and cell integrity on sapphire was confirmed by Fluorescence microscopy as in (**a**) – scale bar 20 microns. IR spectra and its derivative (**b**) indicate several peaks of interest in the laser range (2500-3100cm^{-1}) present in the spectral derivative (1-4).

In this work we exploited a combination of IR absorption nanoimaging and topographic data, which enabled the chemical analysis of sub-50nm resolution-resolved membrane boundaries, label free localization of nuclei and the production of subcellular chemical complexity maps. As many cell processes related to disease are governed by the position and dynamics of subcellular features [22], we utilized the chemical complexity maps to quantify the nanoscale biochemical inhomogeneity of cancer cells with a view to understanding the subcellular biomechanics underlying carcinogenesis.

2. Experimental

Choice of Source

For single wavelength applications, high quality lasers are essential for artefact free imaging [23]. Specifically, for IR nanospectroscopy the laser must have a suitably narrow linewidth, a low signal-to-noise ratio (SNR), and ideally be compact [24] with wide spectral tuneability [25]. Our studies were performed using a pulsed 2KHz repetition rate benchtop Optical Parametric Oscillator (OPO) laser using a 1064nm pump with both near and mid IR tuneability with a 4nm average linewidth for the wavelength range used (2500-6900cm^{-1}). The laser average power was 4mW with pulses of c.a.10ns peak power duration with a focused 0.01cm spot diammeter.

Image Aquisition

The AFM was operated in contact mode using silicon nitride tips mounted on a V-shaped cantilever with a nominal spring constant of 0.05 N/m. A force setpoint of 2 - 5 nN was applied. A Stanford SR650 (Sunnyvale, CA, USA) programmable filter was used to amplify the AFM output. The signal was routed to an oscilloscope (Agilent Inc., Santa Clara CA, USA). The AFM tip deflection was averaged every 16 - 256 laser pulses (before being sampled) to increase the signal to noise, depending on laser stability. The effective spatial lateral resolution was limited by the tip-surface area and the scanning and sampling rates, yielding lateral resolution below 100nm [26], although the depth resolution is significantly larger. The beam was directed upward using gold coated mirrors into a lens which focused the laser light towards the sample, typically to a 50-100μm spot size. Nanoscale IR spectroscopy of samples is performed by detecting the local displacement of the tip by thermally induced dilation of the surface topography [16]. As the wavelength of the IR laser source is tuned into resonance with a vibration mode of the sample chemical species, absorption of IR radiation increases [15].

Culture

Sapphire was chosen as a substrate (UQG Optics, Cambridge) due to its insolubility and linear absorption response across the laser range. The substrates were sterilized by autoclaving and placed into a 6 well plate. A human colon adenocarcinoma cell line (SW480) at a concentration of 10^6 cells/ml was seeded in the wells with 2 ml DMEM medium and incubated at 37° C in a 5% CO2 atmosphere for 24 hours. Flow cytometry of the SW480 cells showed high viability (96.8%) for the culture used for spectral analysis. The integrity of the nuclei and membrane as well as cell adhesion to the sapphire substrates was assessed with fluorescence microscopy (Zeiss AxioImager M1) as in Figure 1(A), which indicated monolayer growth. An unstained sample was selected for FTIR (Agilent, 600 series Santa Clara, CA) of the bulk. FTIR spectra (Figure 1B) illustrated the presence of four absorption bands (2851cm^{-1}, 2872cm^{-1}, 2925cm^{-1}, 2956cm^{-1}) which have all previously been associated with lipids and proteins [27] due to the presence of methylene groups.

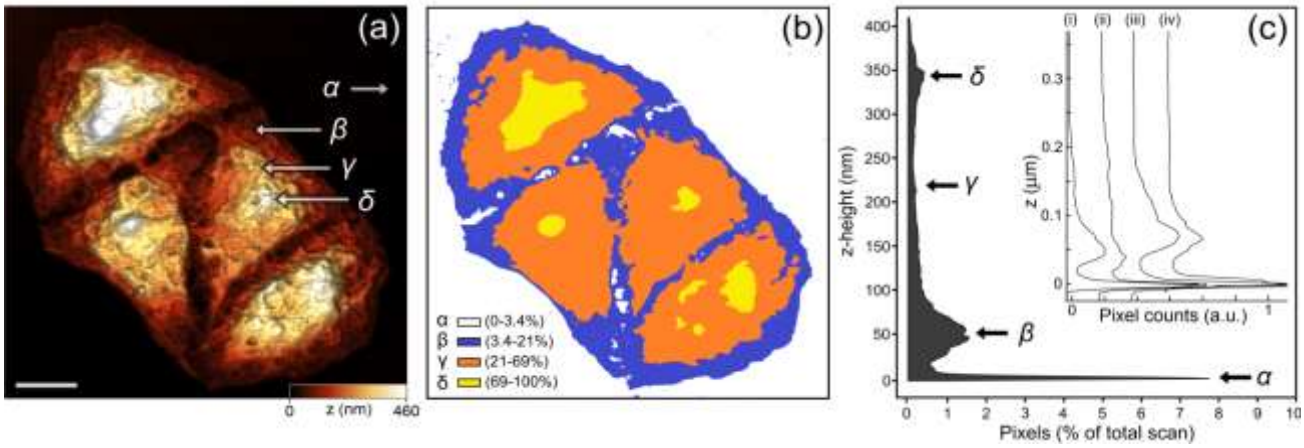

Figure 2 Topographic analysis. The highest point in a cell's topography or any arbitrary choice of height contour does not necessarily correlate to its nucleus. In (**a**) the AFM topography shows a collection of columnar colon cancer cells with overlapping membranes (labeled β) on the substrate (scale bar 10 μm). (**b**) The same area with the four main topographic boundaries color coded as a percentage of cell height. The cytoskeleton and background are coded blue and white respectively. Contour regions which correspond to cytoplasm (orange, γ) are below the uneven, highest topographic features (yellow, δ). In (**c**) we see the height distribution for a cell, with the substrate (α), membrane (β), cytoplasm (γ) and top features (δ) indicated as a percentage of the total scan pixels. The inset (i-iv) shows the height distribution similarity for four cells.

3. Results

AFM analysis

Analysis of cell morphology and profile was performed using AFM. The objective was to assess whether height alone is sufficient as a discriminant of subcellular features. Figure 2A shows a typical shaded topography of columnar colon cancer cells. The image was divided based on four height regions (labelled α, β, γ, δ in order of increasing height). Figure 2(B) shows the four boundaries colour coded as a percentage of cell height The boundaries of these regions, defined as the percentage of maximum height, was iteratively changed and compared to the known cell boundaries found by fluorescence staining of the nuclei and mitochondria. Good agreement was found for the outer membrane boundary at β_{min}=3.4% (Figure 2C) however no choice of the γ and δ height cutoff agreed with the four nuclei boundaries determined by DAPI staining.

This is consistent with the fact that the highest point in a cell's topography does not necessarily correlate to the cell nucleus, but may simply indicate another cell feature such as a clustering of organelle mass. Despite its capacity for nanoscale resolution imaging, the inability for contour isolation of substructures is clearly a limitation on the use of AFM height measurements alone for discriminating subcellular features. This limitation is further compounded by the inherent cell-to-cell variation in morphology [27] such as in Figure 2(C i-iv) which shows the height distribution for four different cells, but also the variation in the population. The substrate is easily recognized as it is evident as a dominant sharp peak (α), which is defines the lowest point in the height distribution

Infrared nanoscopy

Previous studies have indicated that infrared nanospectroscopy of cells is spectrally accurate, and can be correlated with results from conventional FTIR [14]. Examination of a cell subregion, specifically, an area containing both membrane, cytoplasm and nucleus was undertaken in order to probe nanosized features, as shown in Figure 3(A). Analysis of a cell subsection permits visualization of finer topographic features, and also serves to highlight the sub-diffraction limited resolution of the method. Inspection of the image shows a general trend of increasing height moving away from the edge of the plasma membranes towards the centre of the cell.

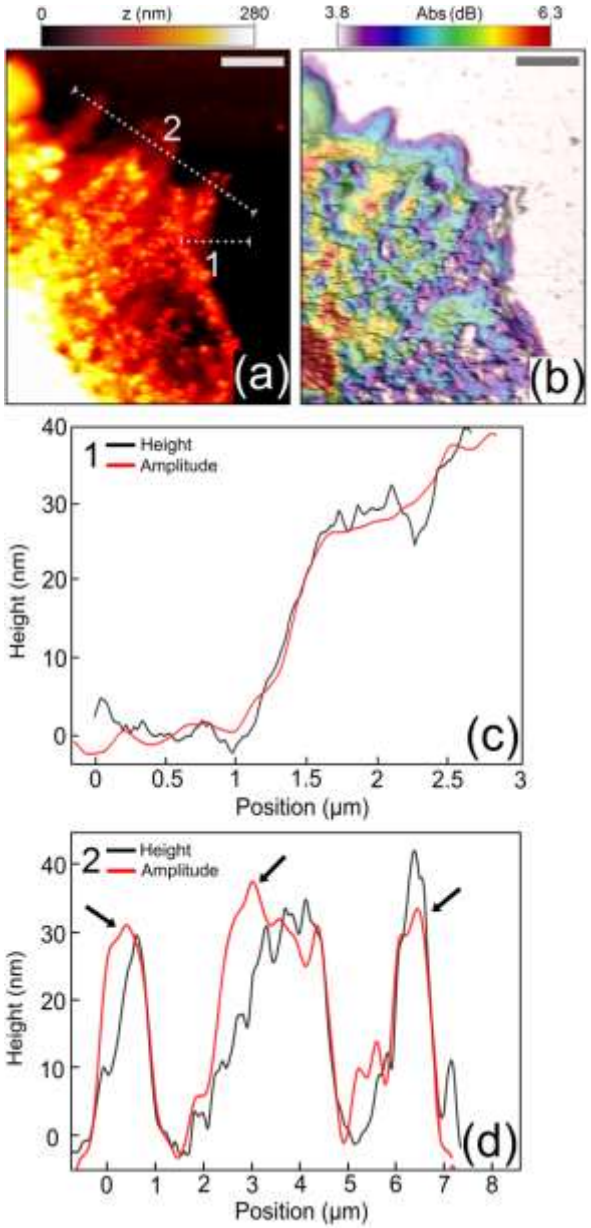

Figure 3 (**a**) AFM measured topography of a cell subsection with the two line profiles (indicated 1,2 shown in C and D), scale bar 3 microns. A shaded topography-absorption overlay is shown in (**b**). Here, morphology is described by shaded topography (such as with real objects) whereas chemical composition, in this case a single wavelength infrared map, is indicated by the color. For chemically homogenous regions, the cell topography and absorption profile are coincident as a function of position, as shown in (**c**). However, where there is more than one chemical species present, the absorption coefficient changes as a function of position, which is observed as a deviation of the IR absorption intensity from the topographic profile (**d** - black arrows). In this way, correlating height and absorption signal can indicate regions of chemical heterogeneity and the presence of multiple chemical species.

The relationship between the infrared signal and the physical properties of the sample has been described in previous work for chemically homogenous materials. These results indicated that for simple homogenous materials such as protein thin films [18], the infrared signal is strongly correlated with the sample height above the background. However, there is a theoretical precedent on the micron scale for the signal dependence on volume, as opposed to specifically on density which would be the more logically intuitive factor influencing absorption. Therefore resolving this issue requires analysis of heterogeneous materials in the context of simpler homogenous analysis, which we now discuss.

Figure 3B shows the corresponding IR absorption map recorded simultaneously with the AFM image. Here morphology is described by shaded topography whereas chemical composition, in this case a mapping of the 2960cm^{-1} absorption peak, is indicated by the colour. As with the topographic signal, there is a general trend of increasing absorption towards the centre of the cell, an observation which agrees with prior line profile comparisons for homogenous materials [17]. However there is local complexity in the relationship between absorption and topography.

For chemically homogenous regions, the cell topography and absorption profile are coincident as a function of position, as shown in Figure 3(C). However, where more than one chemical species is present, the absorption coefficient changes as a function of position, which is observed as a deviation of the IR absorption intensity from the topographic profile (Figure 3D). We note that this variation cannot be accounted for by inherent noise in the measurement as if this was the case, deviations of the IR absorption from the profile would occur universally rather than for distinct, selected cell features. Additionally, the IR signal (averaged here every 256 peak deflections) of homogenous samples does not show similar hotspots and deviations [17]. Examining the relationship between cell topography height and absorption enables assessment of chemical heterogenity. This is because absorption scales with the volume of the material contributing to the IR signal [21] only if the material is homogeneous i.e. if it is comprised of consistent biochemical species, possessing in this case a C-H density that correlates with the band analysed.

Signal Analysis

Before detailing the signal analysis, it is important to note several specifics of the data handling. High quality IR spectroscopy at the nanoscale is sensitive to a range of demanding linear calibrations. These primarily involve calibration of the source intensity as a function of wavelength, beam profile, position and time. The dependence of the incident light intensity, I on output wavelength was monitored using a PbSe Fixed Gain IR Detector (Thorlabs, UK, Ely) which in turn has its own dimensionless spectral response, M(λ). Therefore for, *n* pulses, the absorption coefficient in terms of the maximum of the Fourier Transform (FT) of the cantilever deflection response $V = f_{\max}(v)$ is described proportionally by

$$\alpha(\lambda) \propto \frac{1}{n}\sum_{i=1}^{n} \frac{(V_i(\lambda) - V_0)M(\lambda)}{(I(\lambda) - I_0)} \quad (1)$$

Here we note that the relationship between tip deflection and FT spectral peak is logarithmic and I_0 is the IR detector dark current and V_0 is the background amplitude of the transformed peak. The laser spot size can be easily determined from a digital microscope video of the tip via a visible tracer which is assumed to be Gaussian. The precise beam profile can also be ascertained by acquiring the absorption signal of a blank substrate.

As the AFM raster scans the image area, the readout is a 1D vector which needs to be reshaped into a square matrix in order to be visualized. Time synced masked raster regions were employed in order to correlate the IR and AFM datasets. Image colouring was performed using the Gwyddion software package. The colour coding used was chosen in order to maximize the detail of cell surface features in good contrast but gives little information about the noise and signal from the substrate, which is less experimentally relevant for this work. Cantilever response co-averaging is required for good signal, and also reduces image noise. After analysis, the infrared images were post-processed using a conservative 2D-median filtering algorithm in order to reduce the level of single pixel errors.

Figure 4(A) shows a plot of the PTIR absorption at 2960cm^{-1} as a function of height index for a sample area including both cytoplasm and nucleus averaged every 400 height index points. Here, we define height index as the dimensionless 1D vector of indices associated with the sorted heights in the image, such that the IR absorption values are sorted by height.The dotted line represents linearity, which shows a surprising level of agreement given the absorption dependence on volume, and that the deflection is recorded logarithmically. This implies that the choice of recording either FT peak maxima or raw deflection maxima does not significantly influence the resulting image features. We note that the absorption explicitly depends on the sample height and density associated with the region of tip contact. It is therefore significant that the absorption signal deviates more from the topography at higher, nucleic regions. This is consistent with the understanding that cell nuclei are more chemically complex than the cytoplasm.

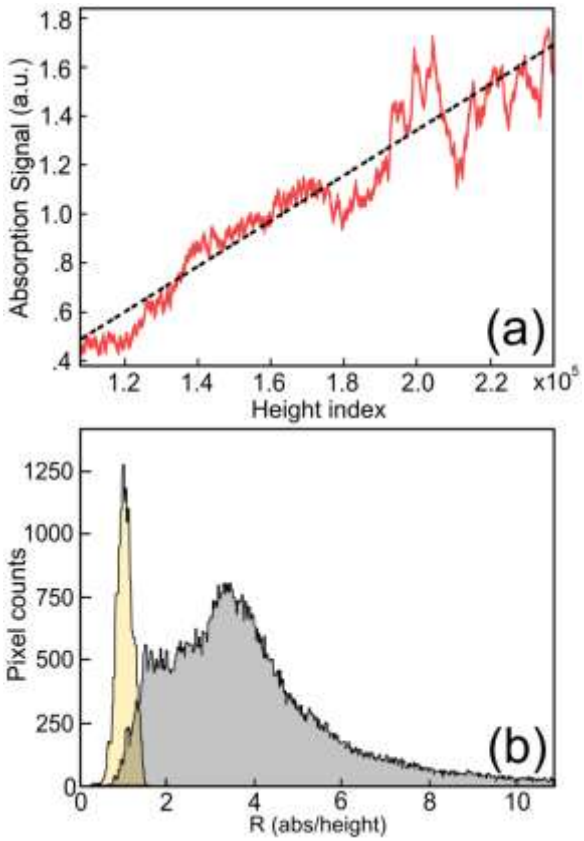

Figure 4. In (**a**) the IR signal is plotted as a function of height index for a 470x470 pixel scan area including both cytoplasm and nucleus (averaged every 400 height index points). A greater variation of the absorption signal from the topography is evident at higher, nucleic regions. (**b**) The distribution of values obtained for the ratio of absorption amplitude to normalized height. Ratio values from the nucleus are presented in yellow whereas the rest of the cell is shown as grey. Although the nucleus exhibits higher IR absorption values (Figure 3), it absorbs less (0.75-1.6) as a proportion of local z-height than the rest of the cell (1.6-10).

Another way to represent this is to observe the distribution obtained for the ratio of absorption amplitude to height shown in Figure 4B. Both height and absorption are have been renormalized with ranges from zero to unity. The ratio values from the nucleus are presented in yellow whereas the nucleus and cytoplasm are counted in grey. The precise border of the dominant nucleus peak was found by multigaussian peak fitting of the ratio histogram. Although the nucleus exhibits higher IR absorption values (Figure 3), it absorbs less (0.75-1.65 vs. 1.5-10) as a proportion of local *z*-height than the rest of the cell. This reduction implies a lower chemical density of absorbing species at 2960cm^{-1} for the nucleus. We attribute this to the dominant absorption of lipids rather than proteins over the broad 2930cm^{-1} absorption band.

These results indicate that the nucleus is distinguishable in height-normalized absorption maps based on two factors; the increased chemical heterogenity evident on its surface (Figure 4A) and the relatively low absorption of the nucleus as a proportion of local *z*-height compared to the rest of the cell (Figure 4B). The ratio map defined over the raster scanned area is

$$R = a \circ z^{\circ(-1)} \tag{2}$$

Where $\circ$ is the Hadarmard product and a and z define the normalized IR absorption and height matrices respectively. Visualization of R, as in Figure 5(B), can be performed by a false colour map of the ratio value at each point of the raster scan, for example using the contrast defined in Figure 5(A). Physically, the laser pulse frequency and cantilever ringdown time can be chosen to be less than the AFM z-piezo feedback response. In this way, the two signals can be present in different frequency regions of the output. This permits the components of the ratio map, absorption and height, to be read simultaneously and without interference. The minima and maxima used are defined by the data ranges, and serve to scale the data so as to rule out unequal weighting in favour of either variable.

Quantifying Nanoscale Heterogeneity

A prominent nucleus peak is indicated by the lowest, red peak in the histogram (Figure 5A). The membrane regions exhibit on average more absorption per unit height than the nucleus with a range from $2 \le R \le 10$ that demonstrates a complex, multipeaked behaviour which we tentatively attribute to the presence of both hydrophobic and hydrophilic membrane regions.

The ratio values present in the background are far larger because although the absorption is low ($T \approx 78\%$), z is defined as near zero at the substrate height. We measure the cell connectivity quantitatively by Minkowski functional analysis of the images [28], which measures local structural propeties and has been succesfully used to measure local properties of nanostructures [29]. This function represents a measure of the interconnectivity of the dataset. For a height normalized IR map, a sharp peak in connectivity corresponds to a strong correlation between the IR absorption and height profiles. Similarly, regions containing large deviations in profile are said to be poorly connected. The actual peak magnitude is depends on the proportion of each species in the scan area, however the peak width also indicates heterogeneity.

Analysis of the Minkowski connectivity confirms several interesting trends (Figure 5C), such as the connectivity of the background (>9.5), which is expected for sapphire. It also displays a 'two tier' behaviour of the membrane with regions of both high and low chemical heterogeneity present. The nucleus displays a broad and prominent reduction in connectivity.

In this way, monovariate infrared imaging can permit a measurement of biochemical heterogeneity. In fact, the emphasis on combined topographic-absorption maps for just one wavelength highlights the degree of local complexity already inherent in a single wavelength map, a fact that could be overlooked in a multivariate study. However we note that a full understanding of precisely which chemicals are present at each location would require detailed multivariate analysis, which should be explored in future work. Additionally this study is spectrally limited from the range of the laser source.

3. Discussion

The application of combined AFM-PTIR data analysis to biological systems has been demonstrated by probing cancer cells with PTIR nanoimaging and performing absorption to height ratio map of the images obtained. These studies indicate that while complex biological systems can be chemically probed with this method, the actual deflection observed is not only a function of the material absorption coefficient, but also of the amount of the absorbing material that is present in the vicinity of the tip [21]. This is likely a significant contributor to the intensity variation observed in previous studies when imaging the same region at different wavelengths [18-21]. Further to this we illustrate that a combined topographic-IR analysis not only permits chemical discrimination on the nanoscale, but can also give insight into chemical heterogeneity at sub-optical diffraction limited resolution.

It is plausible given the current rate of research into the PTIR methods that future studies will extend past 2D multispectral imaging into 3D localization and chemical discrimination of subsurface features, in fact subsurface localization of nanostructures in cells has already been reported [14]. A key step on the way to realizing this is to fully quantify the influence of height on the absorption signal. We provide this study as a further [26] attempt to quantitatively describe the influence of 'z' in PTIR based imaging with a view to potential future studies in 3D nanoscale chemical mapping, but also as a point of reference in understanding the nature of surface chemical homogeneity of cancer cells on the nanoscale.

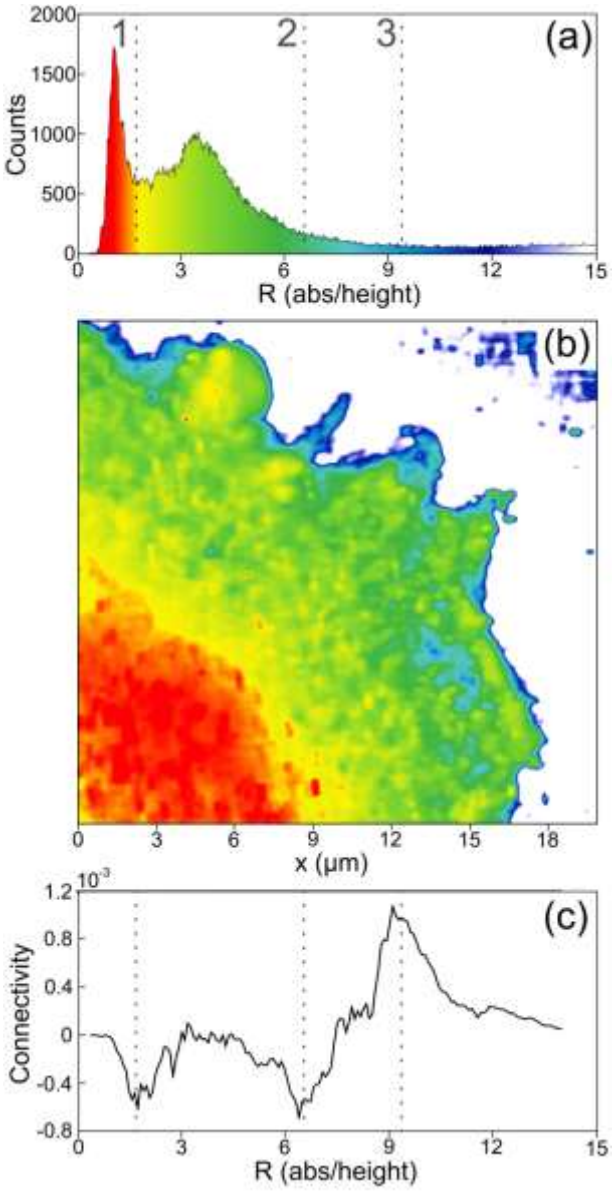

Figure 5 (**a**) Colour coding used for the ratio of absorption amplitude to normalized z-height. The boundaries indicated are for the nucleus (red-1.65), endoplasmic membrane (6.55 - green) and the plasma membrane (blue-9.5). The false colour coding applied to a typical subcellular scan area is shown in (**b**). In this way, combining information from the topography and PTIR greatly enhances the image clarity, permitting chemical localization of the nucleus (1) without the need for pre-treatment or fluorescent labelling. The membrane outer perimeter (at 3) is defined at sub 50nm resolution with an SNR of 61. The Minkowski connectivity (**c**) of the cell's mapping confirms the high connectivity (homogeneity) of the background, the 'two tier' behaviour of the membrane and the chemical heterogeneity of the nucleus.

In this respect the primary observation made is the need for further work to define the absolute rather than relative chemical image complexity, for example by imaging of multiple cell lines at varying stages of carcinogenesis, and performing a multivariate comparison of their interconnectivities.

Recent advances in morphological and cell image analysis for biomedical engineering applications tend to focus on localization, segmentation estimation and modelling of cell parameters. Here we report on the extension a nanometric technique capable of chemical identification which allowed for several unique imaging properties for human epithelial cells including sub-50nm resolution chemically resolved membrane boundaries and label free localization of cell substructures. An assessment of the Minkowksi connectivity for the height normalized absorption images quantified biochemical inhomogeneity in the mammalian cancer calls, which indicated maximum chemical heterogeneity within the nuclei and some membrane regions. This was confirmed against with the expected results from the sapphire background which showed high levels of chemical self-similarity and connectivity.

Several limitations of this method are apparent, the most experimentally prominent being the presence of water which is a strong IR absorber that somewhat constrains the available IR spectral window. However, spectral deconvolution was not necessary in these studies as the primary analysis was performed on single wavelength maps, so the presence of evenly distributed water merely serves a linear offset on the single wavelength absorption intensity. PTIR nanoimaging can also be limited by the possible presence of a contaminant layer on the surface of the sample, which has previously been reported in AFM studies. Such impurities increase the noise on absorption co-efficient measurement due to the contaminants acting as a spatially varying contributor to the deflection. This source of error can be minimized by repeated washing of the surface with PBS and water, which was used as a buffer. Additionally the contaminant layer is assumed to be homogenous and is typically very thin (2-3 nm) compared to cell heights.

4. Conclusion

We illustrate a promising new functionality of PTIR nanoimaging by verifying that sub-diffraction limited infrared microscopy based on photothermal induced resonance, in combination with topographic data, enables several unique imaging properties for human epithelial cells including sub-50nm resolution chemically resolved membrane boundaries and label free localization of nuclei. We outline how by normalizing for cell height, infrared absorption nanoimaging can also quantify local chemical complexity by image analysis with Minkowski functions. In this way, combined AFM-PTIR absorption imaging can uniquely assess and map biochemical inhomogeneity in mammalian cancer cells on the nanoscale. By enabling chemical imaging on the scale of cell substructures we can now probe the biomechanics underlying the structure-function relationship with unprecedented resolution. As PTIR nanoimaging is capable of imaging live cells, it is now possible to explore the role of chemical heterogeneity at varying stages of carcinogenesis.

References

[1] S. Semrau and T. Schmidt, Soft Matter **5**, 3174 (2009).
[2] D. H. Lingwood J. Kaiser, I. Levental, and K. Simons, Biochem. Soc. Trans. **37**, 955 (2009).
[3] D. Kirmizis and S. Logothetidis, Int. J. Nanomed. **5**, 137 (2010).
[4] J. H. Rice, Mol. BioSys. **3**, 781 (2007).
[5] P. Hinterdorfer, M.F. Garcia-Parajo, and Y.F. Dufrene, Acc. Chem. Res. **45**, 327 (2012).
[6] L. Juillerat-Jeanneret, Drug Disc. Today **13**, 23 (2008).
[7] B. D. Hoffman, C. Grashoff, M. A. Schwartz, Nature **475**, 316 (2011).
[8] D. E. Ingber, FASEB J. **20**, 811 (2006).
[9] T. G. Kuznetsova, et al., Micron **38**, 824 (2007).
[10] G. Binnig and C. F. Quate, Phys. Rev. Lett. **56**, 930 (1986).
[11] N. Kodera, D. Yamamoto, R. Ishikawa & T. Ando, Nature **468**, 72 (2010).
[12] I. Sokolov, Cancer Nanotech. ASP **43** 1 (2007).
[13] A. Dazzi, R. Prazeres, E. Glotin, J. M. Ortega, Opt. Lett. **30,** 2388 (2005).
[14] E. Kennedy, R. Al-Majmaie, M. Al-Rubeai, D. Zerulla and J. H. Rice, RSC Adv. **3**, 13789, 2013
[15] J.H. Rice, Nanoscale **2**, 660 (2010).
[16] A. Dazzi, F. Glotin, and R. Carminati, J. Appl. Phys. 107, 124519 (2010).
[17] F. Yarrow, E. Kennedy, F. Salaun, and J. H. Rice, Biomed. Opt. Express **2**, 37 (2011).
[18] E. Kennedy, F. Yarrow, J.H. Rice, J. Biophotonics **4**, 588, (2011).
[19] C. Mayet, A. Deniset-Besseau, R. Prazeres, J. M. Ortega and A. Dazzi, Biotech. Adv. 31, 369 (2013).
[20] C. Mayet, A. Dazzi, R. Prazeres, F. Allot, F. Glotin and J.M. Ortega, Opt. Lett. **33**,1611 (2008).
[21]A.Dazzi, R.Prazeres, F.Glotin, J.M.Ortega, M.Alsawaftah and M.De Frutos, Ultramicroscopy **108**, 635 (2008).
[22] M. Nobis, N. O. Carragher, E. J. McGhee, J. P. Morton, O. J. Sansom, K. I. Anderson and P. Timpson, FEBS J. 2013 DOI: 10.1111/febs.12348

[23] R. F. Curl and F. K. Tittel, Annu. Rep. Prog. Chem., Sect. **C98**, 219 (2002).
[24] F. Lu, Belkin, M. A. Opt. Express **19**, 19942 (2011).
[25]Katzenmeyer, et al. Analytical Chem. **85**, 1972 (2013).
[26] B. Lahiri, G. Holland and A. Centrone, Small **9**, 439 (2013).
[27] J. R. Mourant, Y. R. Yamada, S. Carpenter, L. R. Dominique, and J. P. Freyer, Biophys J. **85**, 1938 (2003).
[28] H. Mantz, K. Jacobs and K. Mecke, J. Stat. Mech. **12**, 12015 (2008).
[29] K. R. Mecke and D. Stoyan, LNP **72,** 554 (2000)